Journal of Fluids and Structures (1997) **11,** 135–158

FLUCTUATING LIFT AND DRAG FORCES ON FINITE LENGTHS OF A CIRCULAR CYLINDER IN THE SUBCRITICAL REYNOLDS NUMBER RANGE

G. S. West and C. J. Apelt
Department of Civil Engineering, The University of Queensland
St Lucia, Qld 4072, Australia

(Received 6 December 1994 and in revised form 30 September 1996)

Spanwise cross-correlations of fluctuating pressures and of elemental fluctuating forces have been measured on long smooth circular cylinders with end plates in the central part of the span where "long" cylinder conditions exist. The data have been obtained at subcritical Reynolds numbers over the range 10^4 to $2{\cdot}1 \times 10^5$ for blockage ratios 0·0425, 0·06 and 0·095 and at turbulence levels of 0·002, 0·0125, 0·03, 0·055 and 0·075. By use of the cross-correlation curves, factors have been calculated which allow the r.m.s. force coefficients for finite lengths of "long" cylinders to be derived from elemental force coefficients. These conversion factors have been applied to previously measured elemental force coefficients to produce coefficients of r.m.s. forces for finite lengths of cylinder up to 50 diameters for the ranges of conditions detailed above.

1. INTRODUCTION

Experiments on long, smooth cylinders in uniform flow reported in West & Apelt (1993) provided accurate data on fluctuating pressure distributions and r.m.s. lift and drag forces on an elemental slice of the cylinder for Reynolds numbers in the range 10^4 to $2{\cdot}5 \times 10^5$. It was established that, provided suitable end plates are used, the r.m.s. lift and drag force coefficients for an elemental slice, i.e. with differentially small length, are independent of spanwise location and of the aspect ratio of the cylinder, A, within the accuracy of measurement, provided $A \geq 10$. Here A is defined as the ratio of the length of the cylinder between end plates, L, to the diameter, D. The "long" cylinder conditions occur everywhere except in regions extending approximately $3{\cdot}5D$ from each end plate where end effects are measurable. In fact, Fox & West (1990) established that "long" cylinder conditions occur at the mid-span section only, when $A = 7$ and similar results are reported by Szepessy and Bearman (1992).

The r.m.s. quantities do not vary with spanwise location in the region with "long" cylinder conditions but, if simultaneous traces of corresponding pressure or force signals from two stations with spanwise separation are compared, it is clear that the instantaneous signals are not the same. In flows with low turbulence and with closely spaced stations, salient features of the trace from one station can be recognized, with a time change, in the trace from the other, indicating a phase shift along the span. With widely spaced stations and turbulent flows, no such relationship is readily apparent although the statistical properties of the signals are identical. Consequently, force coefficients for finite lengths of cylinders are always less than those for an elemental slice because of the imperfect spanwise correlation and use of elemental force

0889–9746/97/020135 + 24 $25.00/fl960070

coefficients for finite lengths of cylinder would result in conservative design. Measurements of fluctuating forces on finite lengths of cylinder reported by Cheung & Melbourne (1983), Kacker *et al.* (1973, 1974), Keefe (1961) and Schewe (1983) have demonstrated this effect but no systematic study of the dependence of the r.m.s. force coefficients on the length has been reported. Spanwise cross-correlation coefficients of the elemental forces can provide such information but, as pointed out by Ribeiro (1992), results for such coefficients reported in the literature are very scarce. Some measurements of spanwise cross-correlations of fluctuating pressure along generators have been reported by Batham (1973), Bruun & Davies (1975), Kiya *et al.* (1982), Novak & Tanaka (1975), Sonneville (1976) and Surry (1972). Szepessy & Bearman (1992) measured spanwise cross-correlations between fluctuating pressure and velocity.

In the experiments reported here, systematic spanwise cross-correlational measurements have been obtained for the fluctuating pressures and for the elemental fluctuating lift and drag forces as functions of the spanwise separation for the regions of cylinders with end plates, where ''long'' cylinder conditions apply. Integration of the spanwise cross-correlation coefficients of the elemental r.m.s. force coefficients, as functions of the spanwise separation, has produced conversion factors which have been applied to the elemental r.m.s. force coefficients to give corresponding coefficients applicable to finite lengths of ''long'' cylinders.

2. EXPERIMENTAL ARRANGEMENT

The equipment, instrumentation and experimental procedures used were the same as those described in detail in West & Apelt (1993); a summary is given here.

Three cylinders of machined and polished brass with diameters 31, 44 and 70 mm were used with end plates sized according to Stansby (1974). The blockage ratio, B, defined as the ratio of the projected area of the cylinder and its end plates to the cross-sectional area of the working section of the wind tunnel had values of 0·0425, 0·06 and 0·095. No blockage correction has been applied to the results because it is considered that no suitable method for blockage correction has been developed for the conditions of the experiments.

Pressures were measured with miniature transducers mounted below the surface of the cylinder. Each transducer communicated with the surface of the cylinder through a 0·5 mm diameter tapping of 1·5 mm length and was calibrated in place for both static and dynamic response. In the studies reported in West & Apelt (1993), 20 pressure transducers were distributed around the circumference of the cylinder at the same spanwise location and the signals from these were processed electronically and integrated on line to given the instantaneous elemental fluctuating force coefficients. The accuracy of measurement of the instantaneous force coefficients in this way is essentially the same as that of the individual pressure measurements, which is better than 1%. For measurements of spanwise correlation of elemental fluctuating forces it is necessary to instrument two cross-sections but it was not possible to use 20 pressure transducers at each section because of limited resources. Studies reported by West (1986) demonstrated that elemental fluctuating forces could be measured with acceptable accuracy by integrating directly on-line the outputs from 10 pressure transducers, provided these were distributed around the circumference of the cylinder in optimal arrangements, one for lift and a different one for drag. The 10 pressure transducers were mounted in a capsule that formed a right cross-section of the cylinder; different capsules were used for measurement of fluctuating lift and drag. Comparison between simultaneous signals from the 20 transducer system and the two 10-transducer

systems installed at the same cross-section of the cylinder showed that the lift and drag signals from the two arrangements were virtually identical; the r.m.s. values agreed within 0·5% and the correlation coefficient between signals was equal to 1 for both lift and drag, in flows with low turbulence and high turbulence. Separately, a dynamometer constructed inside a 1D length of cylinder enabled direct measurement of fluctuating forces on it to be made simultaneously with on-line integration of the signals from 10 pressure transducers installed in the same length of cylinder. The r.m.s. values of the fluctuating lift and drag coefficients measured in these two different ways agreed within 2 and 6%, respectively. It is considered that the accuracy of the force measurements with the 10 pressure transducers is better than is indicated by these figures, which are ''worst'' estimates.

For measurement of spanwise cross-correlations, two pairs of identical capsules each containing 10 pressure transducers were used, one for lift and the other for drag. The spanwise position of the capsules was varied with spacers; the capsules were located symmetrically about the centre-line of the working section and their spanwise separation was varied in steps of 0·5D. The outputs from the pressure transducers in each capsule were processed on-line by two identical instrumentation systems and the outputs from the two capsules were correlated on-line with an analogue correlator.

The wind tunnel was of recirculating type with turning vanes in the four 90° bends and a honeycomb and screens immediately upstream from the contraction leading into the working section. The air speed could be varied continuously up to a maximum of 50 m/s. At the model station the turbulence intensity, u'/U, was 0·2%, where u' in the r.m.s. velocity fluctuations; the velocity distribution was uniform to within ±0·3%. At the largest aspect ratios studied, the end plates were well outside the wall boundary layers.

Turbulent flows were generated by grids mounted upstream of the working section, and the model station was 2750 mm downstream from the grids for the experiments in turbulent flow. Four different grids detailed below were used to produce turbulence intensities of 1·25, 3, 5·5 and 7·5%. With the first grid in place, decay of the turbulence intensity in the streamwise direction was not detectable over distances of order 250 mm upstream and downstream from the model station. With the other grids in place, turbulence intensities were still decaying slowly with distance at the model station. Turbulence intensities of 3% and 5·5% decayed by 1% of their magnitudes over a distance of 60 mm, while the intensity of 7·5% experienced the same relative decay in 40 mm.

At the model station, the time-averaged velocity was uniform to within ±0·5, ±1·8, ±4 and ±5%, and the turbulence intensity was uniform to within ±2·5, ±4, ±5 and ±6% for the four grids, in order of increasing turbulence intensity. The deterioration in the uniformity of the flow parameters at the model station with increase in turbulence intensity is related to the fact that the turbulence downstream from the coarser grids is still decaying at the model station. The spectra of the turbulence were generally similar for all cases, with most of the energy in the range 0–100 Hz and very little above 400 Hz.

Details of the experimental conditions are listed below.

Models. Cylinders, 31·7, 44·4, 69·8 mm in diameter.
End plates. 7D square, with chamfered leading edges; model centreline set 2·5D downstream from the leading edge on the centreline of the plate.
Wind tunnel. 60 kw driven by three axial flow fans in parallel in the return circuit; two variable-speed fans, one fixed speed. Maximum air speed (empty and without

turbulence grids), 50 m/s at a turbulence intensity $T = u'/U = 0{\cdot}002$. Working section 800 mm × 1 200 mm × 3 500 mm long.
Turbulence grids (square mesh), as tabulated below.

Size (mm)	T (%)	s_t (mm)
50×4	1·25	13·5
75×10	3	20
150×30	5·5	34
300×30	7·5	35

The turbulence scale, s_t, is defined as $\int_0^\infty \Lambda \, \mathrm{d}l$, where Λ is the cross-correlation coefficient derived from the outputs of two hot-wire anemometers spaced laterally with separation, l, in the flow at the model station.
Calibration standards. (Static) T.E.M. projection manometer (Betz type). (Dynamic) Brüel & Kjaer $\frac{1}{4}$ inch microphone system.
Pressure transducers. Miniature Gaeltec type $4T$; 5 mm diameter ×20 mm long with 1 mm diameter pressure vent in the curved surface and short-tailed 0·5 mm diameter back vent.

3. CORRELATION COEFFICIENTS

The correlation coefficient for two fluctuating quantities, X and Y, designated, Λ, is calculated as $\Lambda = \overline{XY}/(\sqrt{\overline{X}^2}\sqrt{\overline{Y}^2})$. Λ_p, Λ_L and Λ_D denote the correlation coefficients for the fluctuating pressure, lift and drag, respectively. Correlation coefficients were measured for the attainable ranges of Reynolds number, spanwise spacing between measurement locations, e, and turbulence intensity. The output from the correlator

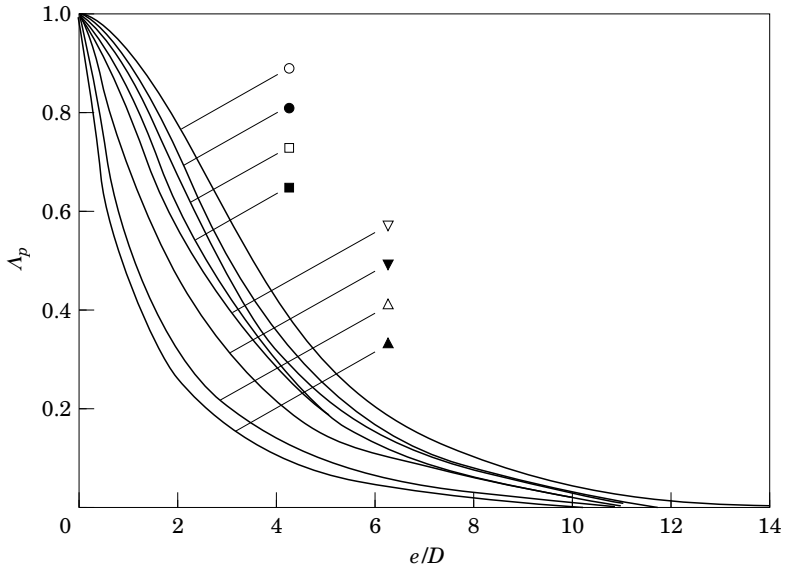

Figure 1. Spanwise cross-correlations of fluctuating pressure in low turbulence flow at $T = 0{\cdot}002$, $A = 35$, $B = 0{\cdot}0425$, $\mathrm{Re} = (2{\cdot}2 - 13{\cdot}3) \times 10^4$ at constant values of θ: ○, $\theta = 27°$; ●, 45°; □, 63°; ■, 72°–117°; ▽, 135°; ▼, 153°; △, 171°; ▲, 180°.

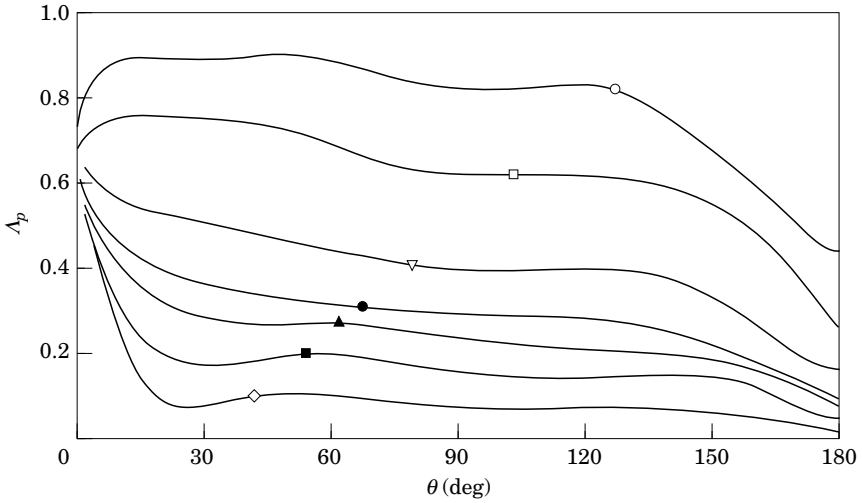

Figure 2. Spanwise cross-correlations of fluctuating pressure in low turbulence flow at $T = 0{\cdot}002$, $A = 35$, $B = 0{\cdot}0425$, Re $= (2{\cdot}2\text{–}13{\cdot}3) \times 10^4$ at constant values of spanwise spacing: ○, $e/D = 1$; □, 2; ▽, 3; ●, 4; ▲, 5; ■, 6; ◇, 8.

was monitored with a pen recorder until it settled to its final, steady-state value after about 2 to 3 min. Though time-consuming, this was found to be an essentially simple and reliable process.

3.1. Fluctuating Pressure Correlations

Since the fluctuating lift and drag are integrals of fluctuating pressures, it was of interest to measure the spanwise correlation of fluctuating pressures at the corresponding angular location, θ, measured from the upstream stagnation point. The signals from individual pressure transducers were considerably smaller than the integrated signals for lift and drag and the signal/noise ratio was less satisfactory, particularly in the vicinity of the stagnation point. Consequently many repeated measurements were made to establish an accurate average value for each individual correlation coefficient and to define correctly the shapes of the correlation curves presented here.

Fluctuating pressure correlations in low turbulence flow and low blockage, $B = 0{\cdot}0425$, are shown in Figure 1. The pressures are correlated best towards the front of the cylinder, and the correlation deteriorates towards the rear. There was no measurable variation with Reynolds number while the flow was in the subcritical range. The same data are presented in alternative form in Figure 2 which shows more clearly the reduction in correlation coefficient as the spanwise spacing and θ increase. The effects of blockage over the range studied were very slight.

The effects of increasing turbulence intensity in the incident flow on the fluctuating pressure correlations are shown in Figures 3, 4, 5 and 6. Changes from the curves for low turbulence become substantial only when the flow exhibits characteristics of the early critical range. When this occurs, the shape of the curves changes and the correlation coefficients decrease noticeably for $\theta > 60°$ approximately; a local minimum appears near $\theta = 110$ to $120°$ with a small local maximum near $\theta = 150$ to $160°$. Increases in turbulence intensity cause these changes to occur at progressively smaller

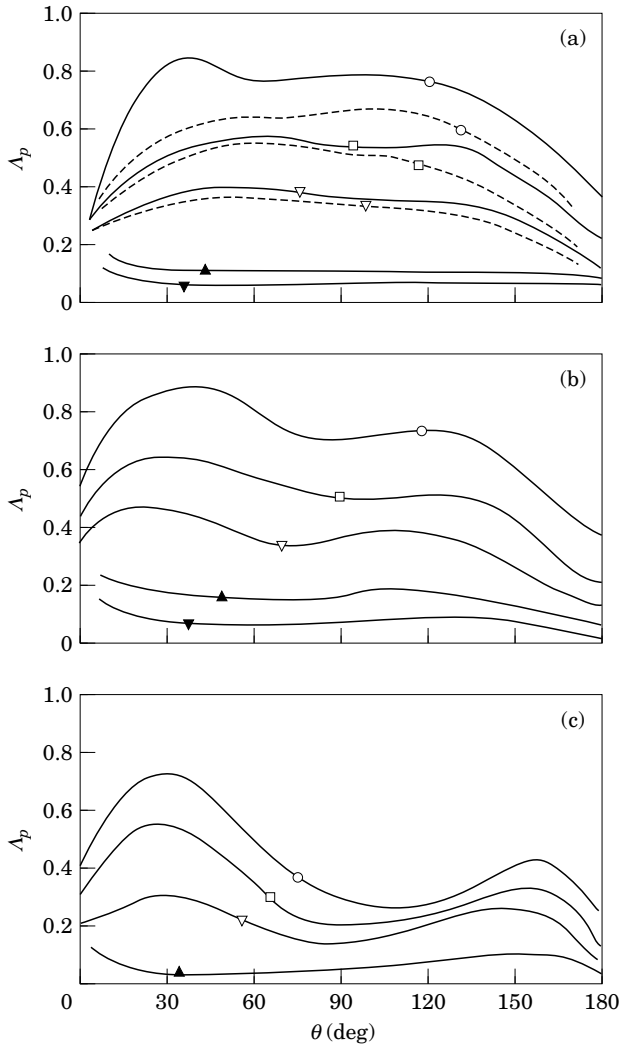

Figure 3. Spanwise cross-correlations of fluctuating pressure at $T = 0{\cdot}0125$, $A = 15$, $B = 0{\cdot}095$. (*a*) - - -, $\mathrm{Re} = 2{\cdot}8 \times 10^4$; ——, $\mathrm{Re} = 5{\cdot}6 \times 10^4$, (b)——, $\mathrm{Re} = (11\text{–}17) \times 10^4$, (c)——, $\mathrm{Re} = 21 \times 10^4$: ○, $e/D = 1$; □, 2; ▽, 3; ▲, 5; ▼, 7.

Reynolds numbers. For $T = 0{\cdot}0125$, $0{\cdot}03$ and $0{\cdot}075$ substantial changes are noticeable at Reynolds numbers equal to $2{\cdot}1 \times 10^5$, $1{\cdot}1 \times 10^5$ and $6{\cdot}6 \times 10^4$, respectively. The variations in the form of the Λ_p versus θ distributions as the flow changes from true subcritical conditions to simulated critical flow can be seen clearly in the sequence in Figure 6, for $T = 0{\cdot}075$. The final set of curves at $\mathrm{Re} = 7{\cdot}7 \times 10^4$ shows the expected low correlation downstream from separation, but there are relatively small effects for θ less than about 45°. Correlation coefficients near $\theta = 0°$ are actually larger than in subcritical flow.

Only limited comparison can be made between these results and those published by others because of differences in experimental parameters and/or lack of details about them. Surry's (1972) data for lateral scales of fluctuating pressures, s_p, for his case *O*, for which T is 2·5%, $B = 0{\cdot}039$ and Re is $4{\cdot}42 \times 10^4$, are compared with corresponding

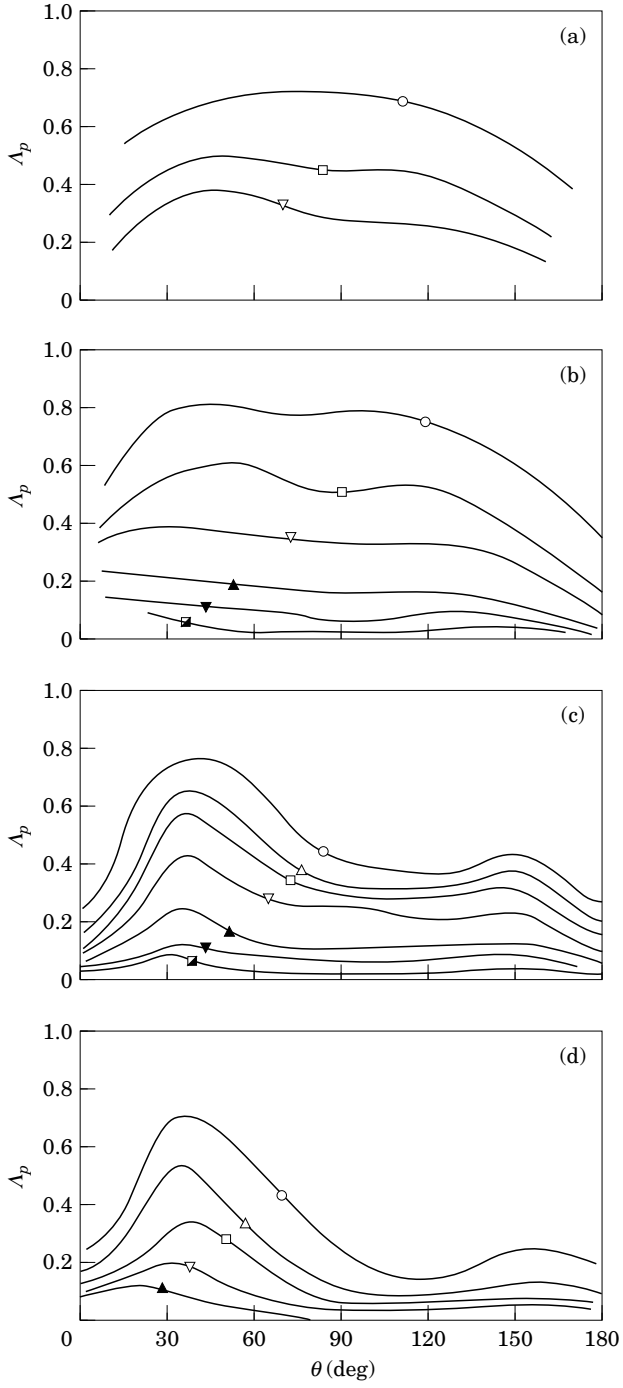

Figure 4. Spanwise cross-correlations of fluctuating pressure at $T = 0{\cdot}03$, $A = 15$, $B = 0{\cdot}095$. (a) $\mathrm{Re} = 2{\cdot}8 \times 10^4$, (b) $\mathrm{Re} = 5{\cdot}6 \times 10^4$, (c) $\mathrm{Re} = 11{\cdot}2 \times 10^4$, (d) $\mathrm{Re} = 14{\cdot}3 \times 10^4$: ○, $e/D = 1$; △, 1·5; □, 2; ▽, 3; ▲, 5; ▼, 7; ◪, 9.

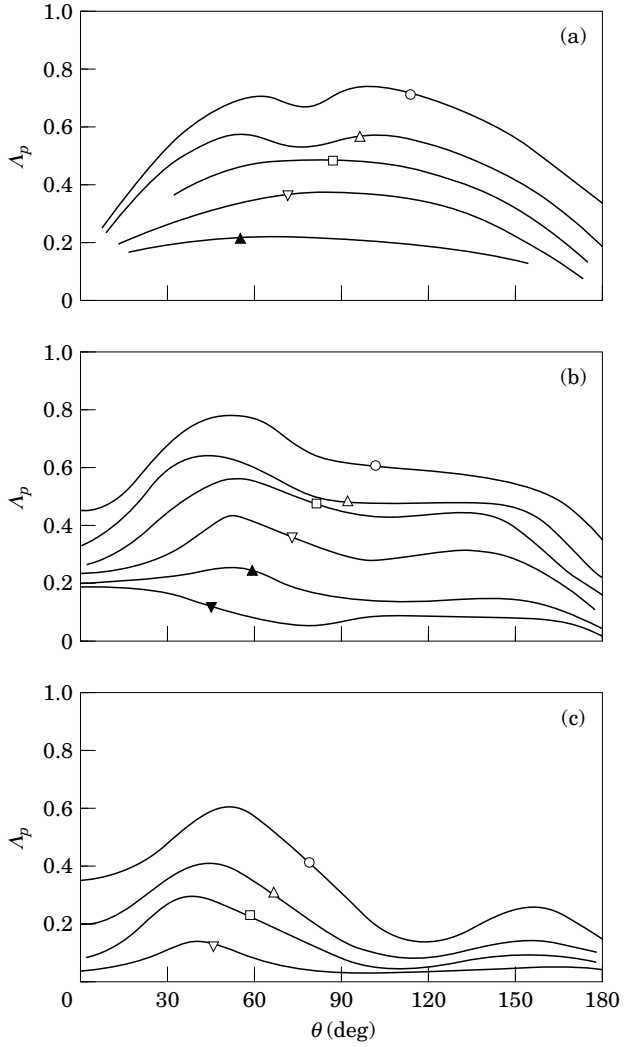

Figure 5. Spanwise cross-correlations of fluctuating pressure at $T = 0{\cdot}055$, $A = 15$, $B = 0{\cdot}095$. (a) $\mathrm{Re} = 2{\cdot}8 \times 10^4$, (b) $\mathrm{Re} = 5{\cdot}6 \times 10^4$, (c) $\mathrm{Re} = 11{\cdot}2 \times 10^4$: Data symbols as in Figure 4.

data derived from Figure 4, for which T is 3% and Re is $5{\cdot}6 \times 10^4$, in Figure 7. The two sets of data are generally similar, and the differences between them are consistent with the deterioration in correlation which occurs with increases in turbulence and with Reynolds number. It is noted that $A = 39$ in Surry's experiments. The data in Figure 4 are also consistent with cross-correlations measured by Bruun & Davies (1975) at $T = 0{\cdot}038$, $B = 0{\cdot}13$, $\mathrm{Re} = 8 \times 10^4$ and $A = 9{\cdot}9$. As shown in Figure 8, the latter results lie between those from Figure 4 at $\mathrm{Re} = 5{\cdot}6 \times 10^4$ and $11{\cdot}2 \times 10^4$ and are consistent with them, showing relatively small deterioration in correlation towards the front of the cylinder and substantial deterioration over the rear part. Szepessy (1991) measured spanwise cross-correlations of fluctuating pressures at 90° from the stagnation point at $T = 0{\cdot}0005$, $B = 0{\cdot}067$, $\mathrm{Re} = 4{\cdot}3 \times 10^4$ and $A = 10$. His results are compared in Figure 9 with pressure cross-correlations extracted from Figure 2. There is good general agreement between the two sets of data which were measured under similar conditions.

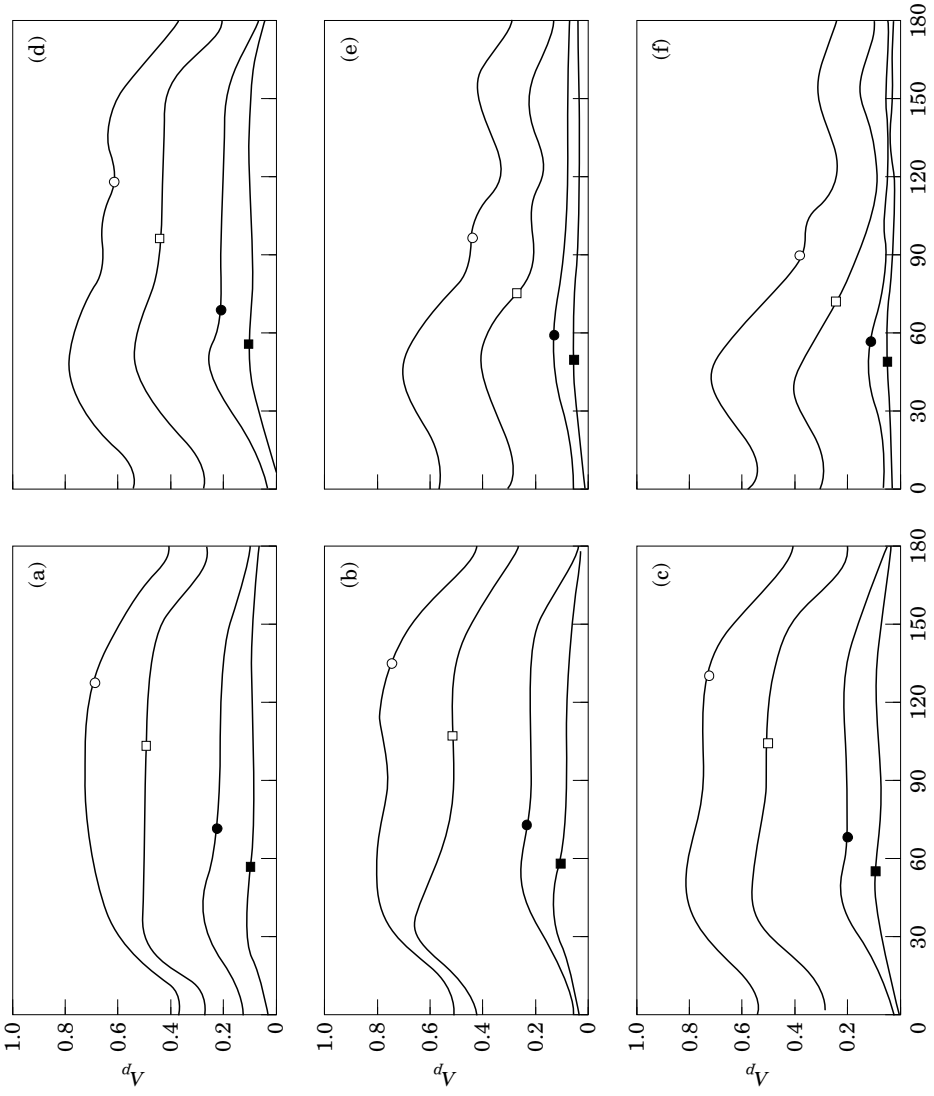

Figure 6. Spanwise cross-correlations of fluctuating pressure at $T = 0{\cdot}075$, $A = 35$, $B = 0{\cdot}0425$. (a) $\mathrm{Re} = 1{\cdot}1 \times 10^4$, (b) $\mathrm{Re} = 2{\cdot}2 \times 10^4$, (c) $\mathrm{Re} = 3{\cdot}3 \times 10^4$, (d) $\mathrm{Re} = 4{\cdot}4 \times 10^4$, (e) $\mathrm{Re} = 6{\cdot}6 \times 10^4$, (f) $\mathrm{Re} = 7{\cdot}7 \times 10^4$: ○, $e/D = 1$; □, 2; ●, 4; ■, 6.

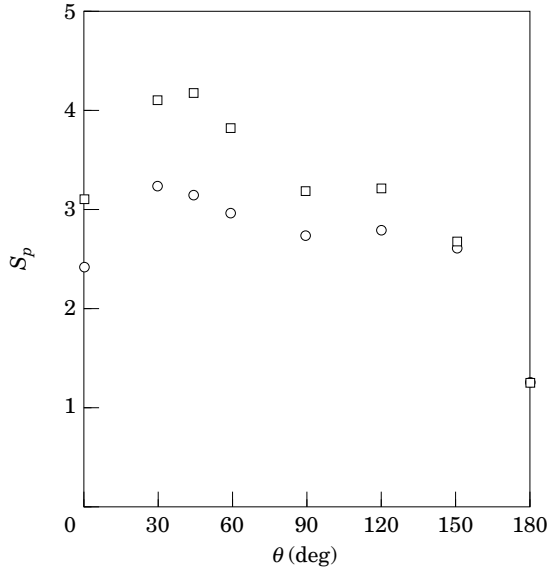

Figure 7. Lateral scales of fluctuating pressure. Comparison with Surry (1972): ⊙, this study at $T = 0{\cdot}03$, $A = 15$, $B = 0{\cdot}095$, $\mathrm{Re} = 5{\cdot}6 \times 10^4$; ⊡, Surry at $T = 0{\cdot}025$, $A = 39$, $B = 0{\cdot}039$, $\mathrm{Re} = 4{\cdot}4 \times 10^4$.

3.2. Fluctuating Force Correlations

The spanwise cross-correlation curves for elemental fluctuating lift and drag forces measured in low turbulence flow for the three blockage ratios are given in Figures 10 and 11, respectively. The fluctuating lift is best correlated at the lower end of the subcritical range of Reynolds number. The correlation deteriorates gradually with increasing Reynolds number, except that for $B = 0{\cdot}095$ the correlation at

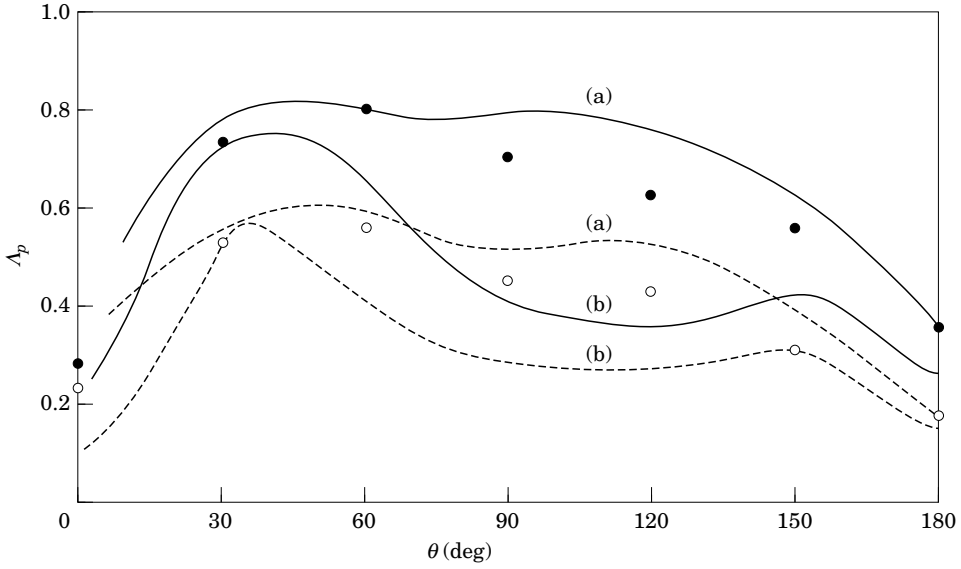

Figure 8. Spanwise cross-correlations of fluctuating pressure. Comparison with Bruun & Davies (1975). This study at $T = 0{\cdot}03$, $A = 15$, $B = 0{\cdot}095$ for (a) $\mathrm{Re} = 5{\cdot}6 \times 10^4$, and (b) $\mathrm{Re} = 11{\cdot}2 \times 10^4$: ——, $e/D = 1$; – –, $e/D = 2$. Bruun & Davies at $T = 0{\cdot}038$, $A = 9{\cdot}9$, $B = 0{\cdot}13$, $\mathrm{Re} = 8 \times 10^4$: ●, $e/D = 1$; ○, $e/D = 2$.

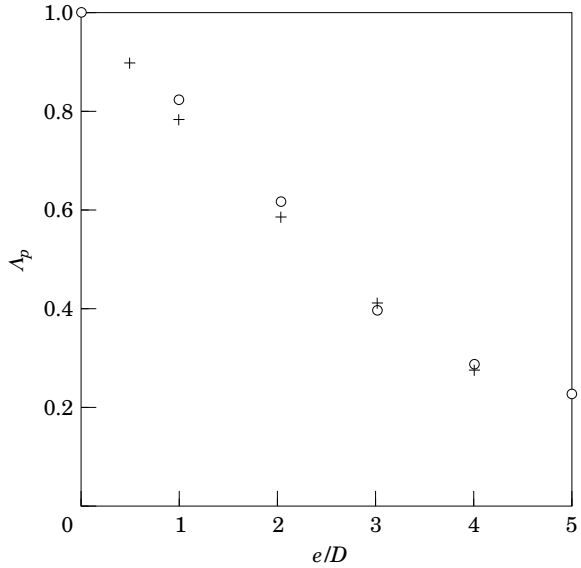

Figure 9. Spanwise cross-correlations of fluctuating pressure at $\theta = 90°$. Comparison with Szepessy (1991): ⊙, this study at $T = 0{\cdot}002$, $A = 35$, $B = 0{\cdot}0425$, $\mathrm{Re} = (2{\cdot}2 - 13{\cdot}3) \times 10^4$; +, Szepessy at $T = 0{\cdot}0005$, $A = 10$, $B = 0{\cdot}067$, $\mathrm{Re} = 4{\cdot}3 \times 10^4$.

$\mathrm{Re} = 2{\cdot}1 \times 10^5$ shows a small improvement. The spanwise correlation of the fluctuating drag is always much worse than that of the lift at the same conditions, but its variation with Reynolds number is somewhat less and, in fact, it improves slightly with increasing Reynolds number over the range tested until some deterioration occurs as Re increases further from $1{\cdot}7$ to $2{\cdot}1 \times 10^5$.

The effects of increasing turbulence intensity in the incident flow on the fluctuating lift and drag correlations can be seen in Figures 12 and 13, respectively, which present results for the largest cylinder at $B = 0{\cdot}095$. In general, the spanwise correlation of fluctuating lift shown in Figure 12 deteriorates with increasing turbulence at the same Reynolds number. As the Reynolds number and or turbulence levels are increased from lower values, the deterioration in the correlation is gradual and relatively small, until at a certain stage there is a large deterioration in correlation as these parameters are increased further. In some cases this deterioration was so rapid that either of two distinctly different values of correlation coefficient could be obtained in repeated experiments at essentially the same conditions. This phenomenon gave rise to the two separate lift cross-correlation curves at $\mathrm{Re} = 2{\cdot}1 \times 10^5$ for $T = 0{\cdot}0125$ and at $\mathrm{Re} = 1{\cdot}1 \times 10^5$ for $T = 0{\cdot}03$ in Figure 12. Apparently, small differences in conditions at Reynolds numbers near the upper end of the subcritical range can result in large changes in the degree of spanwise correlation of the vortex shedding and of the associated fluctuating pressures and forces. In general, the value of Reynolds number at which rapid deterioration in spanwise correlation occurs decreases as T is increased. This is illustrated by the two cases discussed above and, further, by the large change at $\mathrm{Re} = 5{\cdot}6 \times 10^4$ when T increases from $0{\cdot}055$ to $0{\cdot}075$, as shown in Figure 12. The spanwise correlation of fluctuating drag shown in Figure 13 is always much less than that of fluctuating lift for the same conditions, but it shows the same trends with increases in Reynolds number and turbulence levels, apart from the small improvement in correlation as Re increases from $2{\cdot}8$ to $5{\cdot}6 \times 10^4$ at $T = 0{\cdot}0125$ and $0{\cdot}03$.

The general shape of correlation curves for well-correlated quantities is shown in

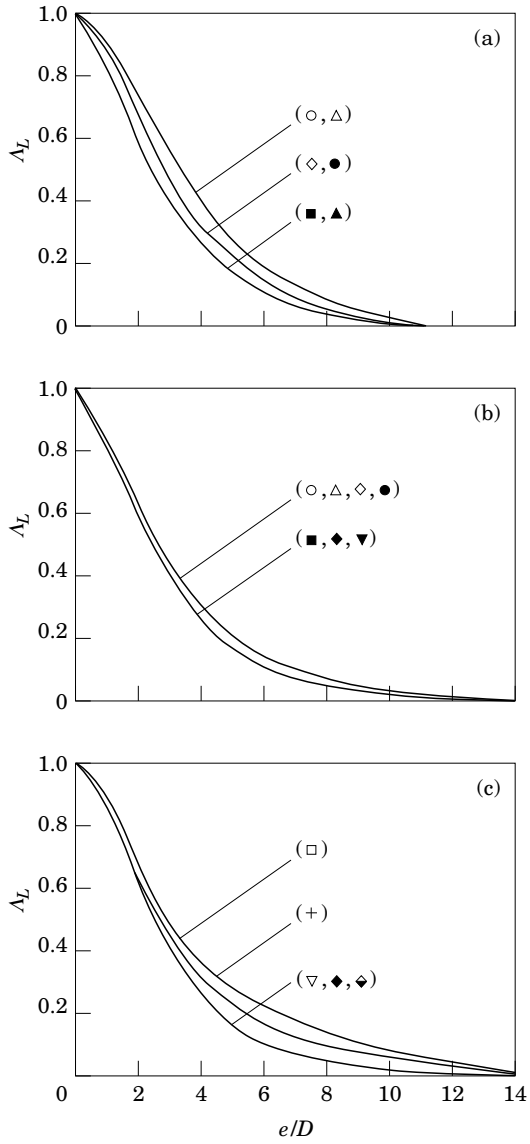

Figure 10. Fluctuating lift force cross-correlations in low turbulence flow at $T = 0{\cdot}002$. (*a*) $A = 35$, $B = 0{\cdot}0425$, (b) $A = 15$ & 25, $B = 0{\cdot}06$, (c) $A = 15$, $B = 0{\cdot}095$: ○, $\mathrm{Re} = 2{\cdot}2 \times 10^4$; □, $2{\cdot}8 \times 10^4$; △, $3{\cdot}3 \times 10^4$; ◇, $4{\cdot}4 \times 10^4$; ▽, $5{\cdot}6 \times 10^4$; ●, $6{\cdot}6 \times 10^4$; ■, $8{\cdot}8 \times 10^4$; ▲, $9{\cdot}5 \times 10^4$; ◆, $11{\cdot}1 \times 10^4$; ▼, $13{\cdot}3 \times 10^4$; ◪, 14×10^4; ⬙, 17×10^4; +, 21×10^4.

Figure 14 as type 1 and poorly correlated quantities tend to the form of type 2. The fluctuating lift is well correlated in smooth flow at the lower end of the subcritical Reynolds number range and as the flow approaches the critical range the correlation deteriorates to produce correlation curves of Type 2. It seems that Type 2 curves for lift are characteristic of flows where the transition from subcritical flow has occurred, or is beginning to take place. As discussed above, it proved difficult to take correlation measurements in the transitional region, whether this was induced by increased Reynolds number or increased turbulence, since the flow can arbitrarily switch from one correlation curve type to the other. In this transitional region before critical flow

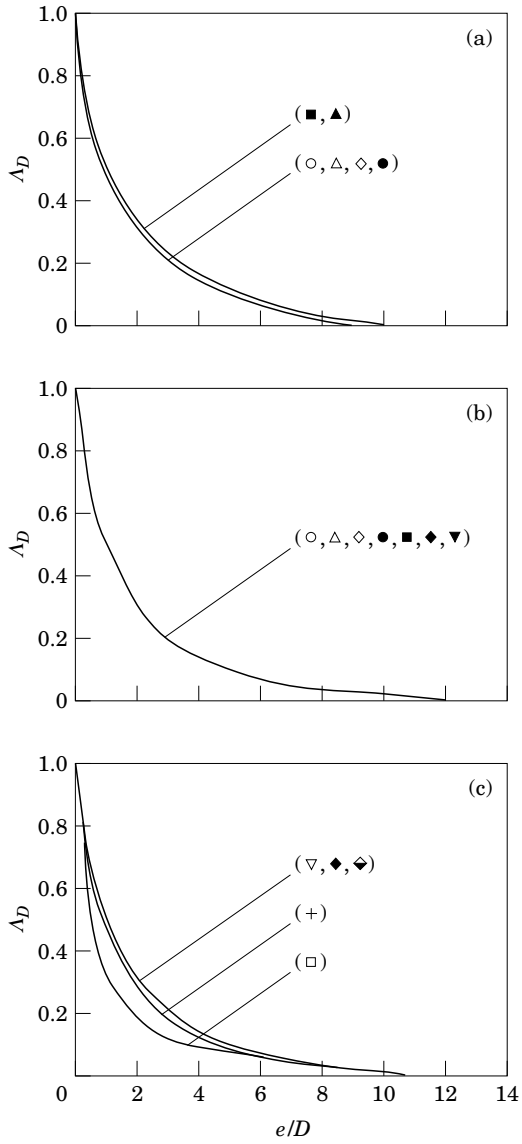

Figure 11. Fluctuating drag force cross-correlation in low turbulence flow at $T = 0{\cdot}002$. (a) $A = 35$, $B = 0{\cdot}0425$, (b) $A = 15$ & 25, $B = 0{\cdot}06$, (c) $A = 15$, $B = 0{\cdot}095$; data symbols as in Figure 10.

has developed fully there is some ambiguity as to whether a particular flow is well- or badly correlated.

4. R.M.S. FORCE COEFFICIENTS FOR FINITE LENGTHS OF CYLINDER

The r.m.s. force coefficients for finite lengths of "long cylinders" can be derived from the elemental r.m.s. force coefficients with use of a conversion factor, f, which is calculated by integration of the cross-correlation curves presented in Figures 10 to 13,

$$f = \left(2\int_0^l \Lambda_F(s)(l-s)\,\mathrm{d}s\right)^{1/2} \Big/ l. \tag{1}$$

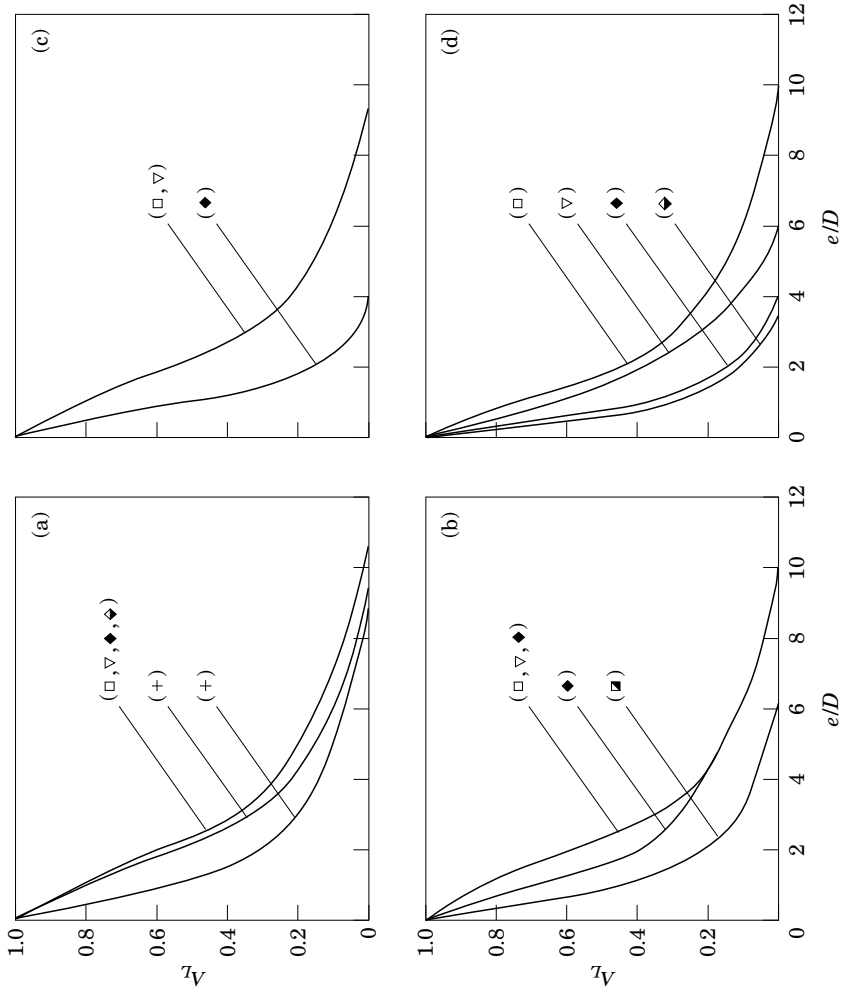

Figure 12. Fluctuating lift force cross-correlations in turbulent flow at $A = 15$, $B = 0{\cdot}095$. (*a*) $T = 0{\cdot}0125$, (b) $T = 0{\cdot}03$, (c) $T = 0{\cdot}055$, (d) $T = 0{\cdot}075$; data symbols as in Figure 10.

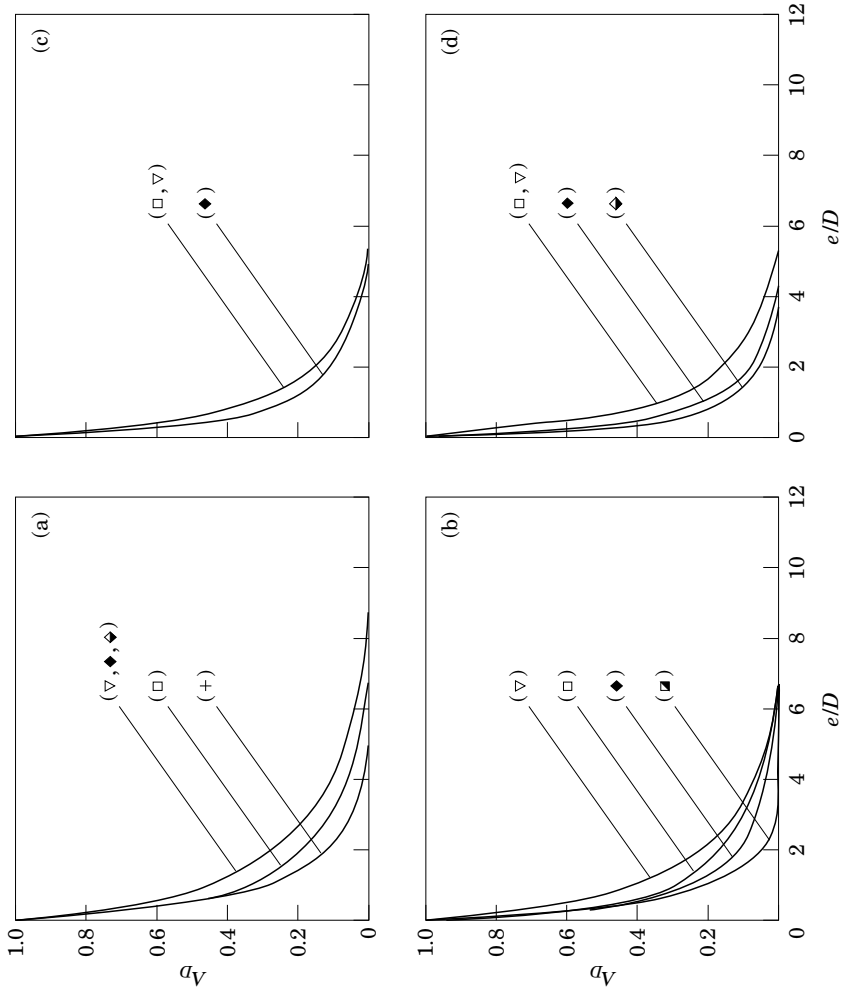

Figure 13. Fluctuating drag force cross-correlations in turbulent flow at $A = 15$, $B = 0{\cdot}095$. (a) $T = 0{\cdot}0125$, (b) $T = 0{\cdot}03$, (c) $T = 0{\cdot}055$, (d) $T = 0{\cdot}075$; data symbols as in Figure 10.

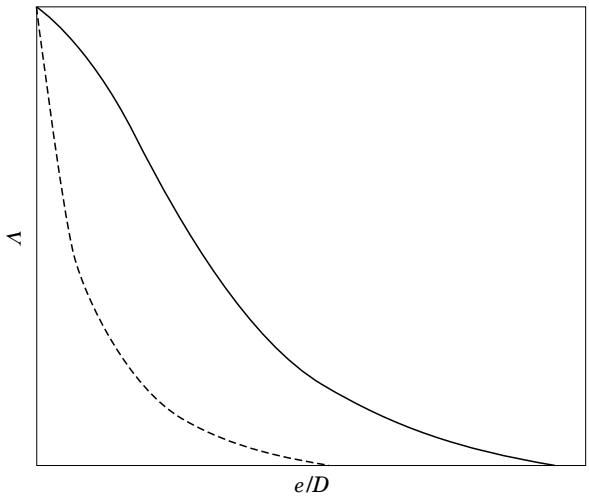

Figure 14. Characteristic spanwise cross-correlation curves: ——, Type 1, well correlated; - - -, Type 2, poorly correlated.

Here, f is defined as the ratio $(C'_F(l)/C'_F(0)$, where $C'_F(l)$ is the r.m.s. force coefficient for a finite length, l, of a ''long'' cylinder, $C'_F(0)$ is the elemental r.m.s. force coefficient, and $\Lambda_F(s)$ is the cross-correlation coefficient of the fluctuating forces on two elements separated by a distance, s. This expression was reported by Frenkiel (1949) and its derivation is also given by Kacker *et al.* (1974) and West (1986).

The conversion factors have been calculated for all conditions tested, by numerical integration of equation (1) using the cross-correlation curves presented in Figures 10 to 13 and others from West (1986). The complete set of conversion factors for the three models tested is given as the curves in Figures 15, 16 and 17. In all cases the conversion factor for fluctuating drag is lower than that for fluctuating lift at the same conditions, reflecting the poorer spanwise correlation of fluctuating drag. The effects on the conversion factors of variations in Reynolds number and turbulence intensity reflect directly the influence of these parameters on the spanwise correlations of fluctuating forces discussed above. The conversion factors have been applied to the elemental r.m.s. force coefficients given in West & Apelt (1993) and West (1986) to give the r.m.s. force coefficients for finite lengths of a ''long'' cylinder which are presented in Figures 18, 19 and 20. These coefficients apply to finite lengths of ''long'' cylinders with end plates, in the region not affected by the end plates, i.e. at least $3{\cdot}5D$ from the end plate.

As expected, the r.m.s. force coefficients for finite lengths of cylinder are smaller than the elemental coefficients and they decrease progressively as the length increases. The relative changes are greatest for l/D in the range 0 to 10; approximately the same reduction in r.m.s. lift coefficient occurs as l/D increases from 0 to 10 as occurs in the range 10 to 50. The r.m.s. drag coefficient decreases even more rapidly with increasing length than does the lift coefficient. The data for C'_L and C'_D in Figures 18, 19 and 20 reflect the combined effects of increases in Reynolds number on the elemental r.m.s. force coefficients and on their spanwise correlation for constant values of blockage, turbulence and l/D. In some cases the variation with Reynolds number is very rapid because of rapid changes in spanwise correlation, as discussed in Section 3.2. The value of Reynolds number at which this rapid transition occurs is reduced progressively as the turbulence in the incident flow is increased. This is illustrated clearly in Figure 20

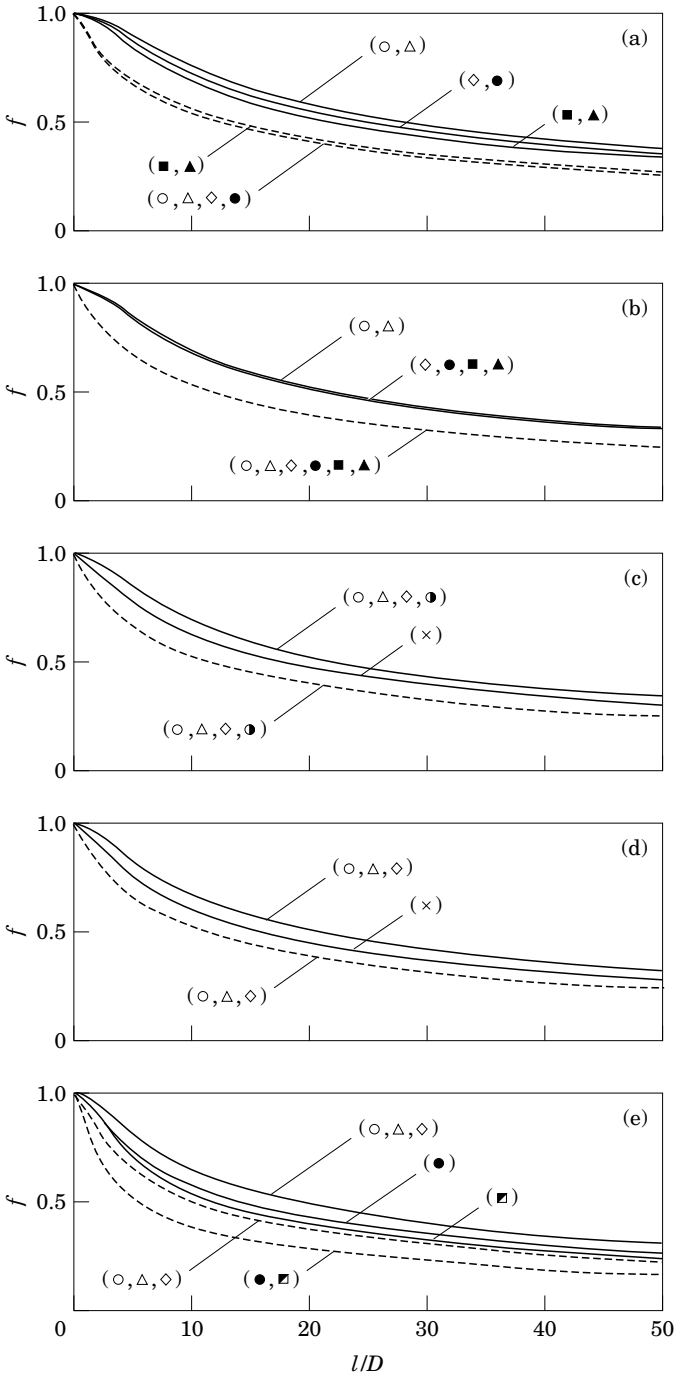

Figure 15. Factors to convert elemental r.m.s. force coefficients to coefficients for finite lengths of long cylinders at $B = 0{\cdot}0425$. (*a*) $T = 0{\cdot}002$, (b) $T = 0{\cdot}0125$, (c) $T = 0{\cdot}03$, (d) $T = 0{\cdot}055$, (e) $T = 0{\cdot}075$: ——, lift; - - -, drag; ×, $\mathrm{Re} = 1{\cdot}1 \times 10^4$; ○, $2{\cdot}2 \times 10^4$; □, $2{\cdot}8 \times 10^4$; △, $3{\cdot}3 \times 10^4$; ◇, $4{\cdot}4 \times 10^4$; ▽, $5{\cdot}6 \times 10^4$; ◑, 6×10^4; ●, $6{\cdot}6 \times 10^4$; ◩, 8×10^4; ■, $8{\cdot}8 \times 10^4$; ▲, $9{\cdot}5 \times 10^4$; ◆, $11{\cdot}1 \times 10^4$; ▼, $13{\cdot}3 \times 10^4$; ◪, 14×10^4; ⬙, 17×10^4; +, 21×10^4.

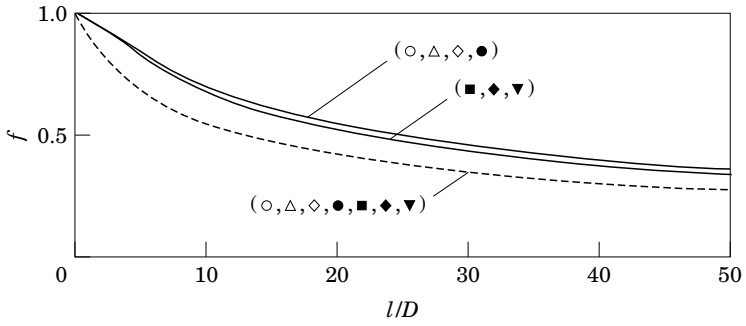

Figure 16. Factors to convert elemental r.m.s. force coefficients to coefficients for finite lengths of long cylinders at $B = 0{\cdot}06$ and $T = 0{\cdot}002$: ——, lift; - - -, drag; data symbols as in Figure 15.

for $B = 0{\cdot}095$, where the Reynolds number at the rapid transition in C'_L is reduced by a factor of approximately 10 as T is increased from 0·0125 to 0·075. The pattern for C'_D is similar to that for C'_L.

Of the limited data published on fluctuating forces on cylinders of finite length only that of Keefe (1961) has been measured in "long" cylinder conditions. Some of Keefe's measurements of C'_L were made on active length $l = D$ at mid-span of a cylinder with $A = 18$ between circular end plates and $B = 0{\cdot}04$, and the results from these tests are compared in Figure 21(a) with the present results for $B = 0{\cdot}0425$ for the case $T = 0{\cdot}002$, since the turbulence in his tests is described as "low". Keefe's results lie close to the present results for $l/D = 5$. They are a little lower than would be predicted from the data in Figure 18. It is possible that the end plates used by Keefe were not large enough and also that there was some leakage at the ends of the active length with which the forces were measured. Each of these would result in a reduction in C'_L below the magnitude for "long" cylinder conditions.

Cheung & Melbourne (1983) report measurements of C'_L for finite lengths of cylinders. They measured forces on the whole length of the cylinder with end plates of size $3D$ wide by $4D$ long. Their results were corrected for blockage with an empirical method they had developed and, so, they are compared with the results for low blockage, $B = 0{\cdot}0425$, in Figure 21(a). The largest value of A was 6·7 and effects due to the end plates would have been present over the whole length. Their results for this case, for which $l/D = 6{\cdot}7$ and $T = 0{\cdot}004$, are compared in Figure 21(a) with the present results for the case of $T = 0{\cdot}002$. They lie close to the curve for $l/D = 5$ and are generally consistent with the data of Figure 21(a) but no more specific inference can be drawn from the comparison since "long" cylinder conditions did not occur.

Schewe (1983) measured the fluctuating lift on a cylinder which spanned the width of the working section without end plates, with $A = 10$, $l/D = 10$, $B = 0{\cdot}10$ and $T < 0{\cdot}004$. His data are compared in Figure 21(b) with the present results for the conditions, $B = 0{\cdot}095$ and $T = 0{\cdot}002$. Schewe's data are close to the present data for $l/D = 10$ at lower Reynolds numbers but diverge from them at higher Reynolds numbers. The conditions in Schewe's experiments would not have produced "long" cylinder conditions. Nevertheless, the large differences in C'_L at the larger Reynolds numbers raise questions about the effects of the free ends of the cylinder. The rapid reduction in C'_L at larger Reynolds numbers is similar to the pattern observed when the cylinder is in the critical range of Reynolds number, but it seems unlikely for this to be the case here.

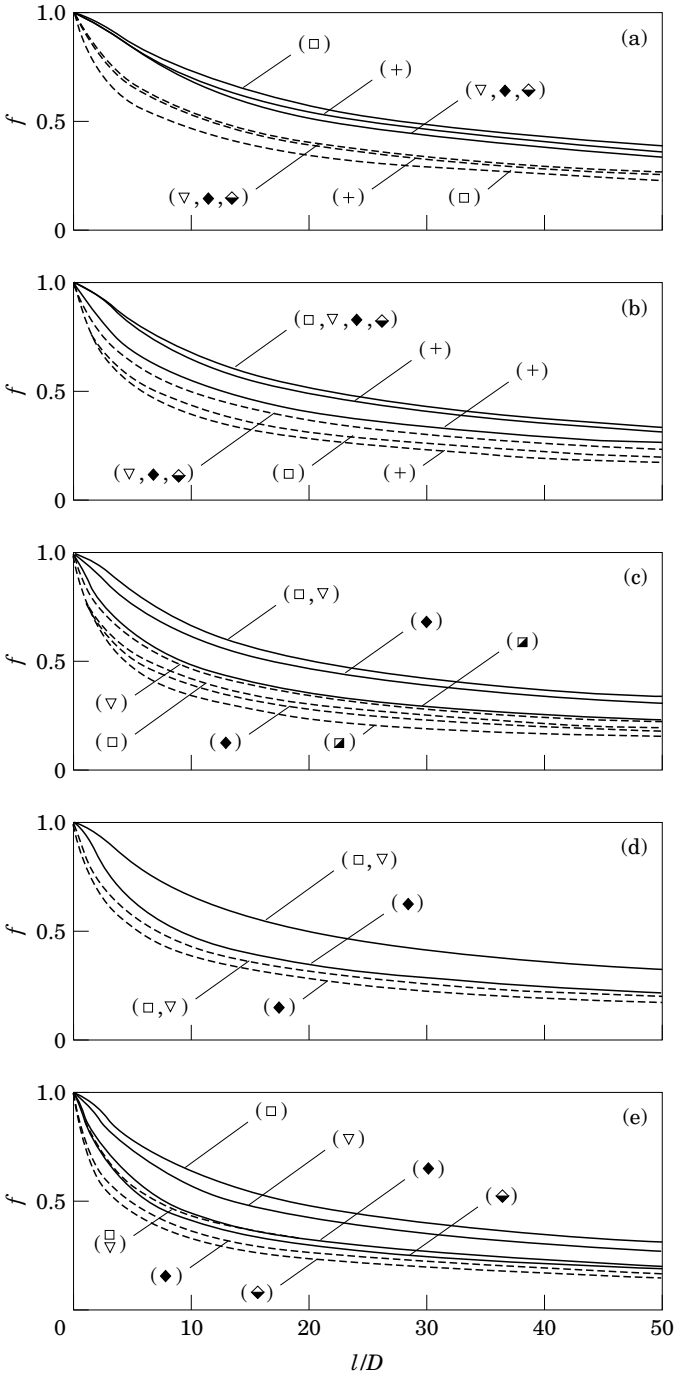

Figure 17. Factors to convert elemental r.m.s. force coefficients to coefficients for finite lengths of long cylinders at $B = 0{\cdot}095$. (a) $T = 0{\cdot}002$, (b) $T = 0{\cdot}0125$, (c) $T = 0{\cdot}03$, (d) $T = 0{\cdot}055$, (e) $T = 0{\cdot}075$: ——, lift, - - -, drag; data symbols as in Figure 15.

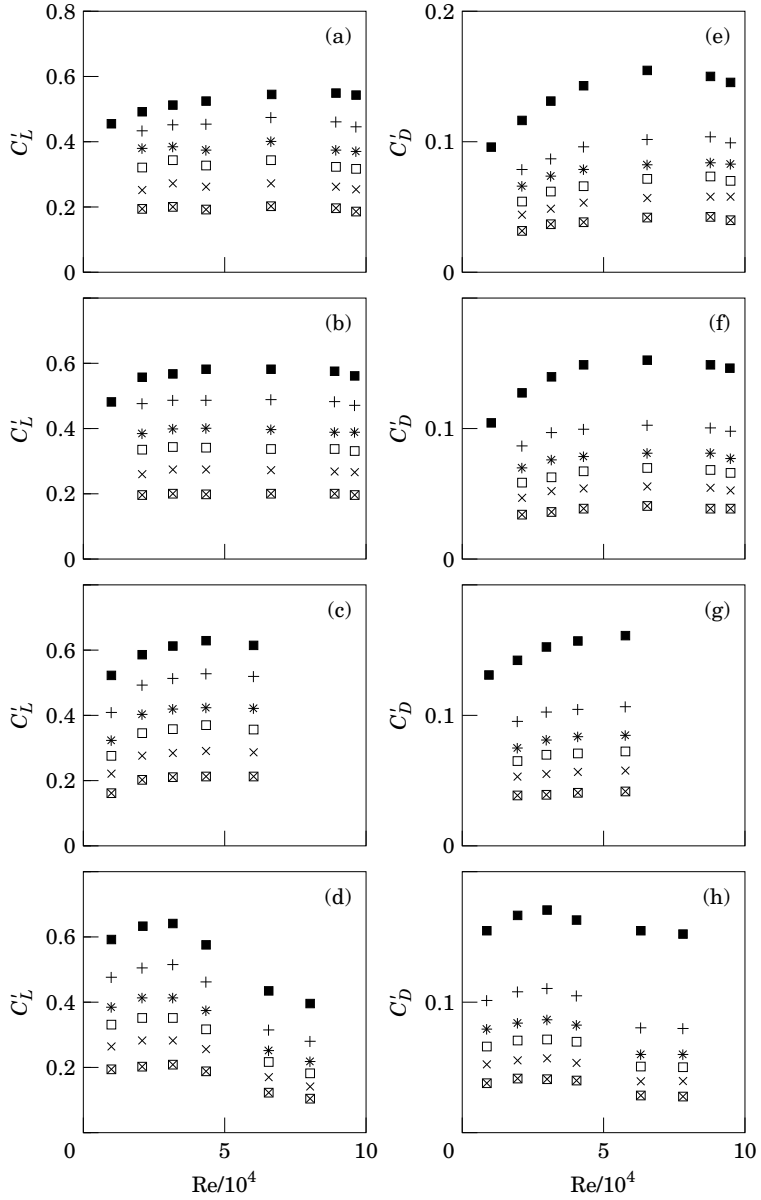

Figure 18. R.m.s. force coefficients for finite lengths of long cylinders at $B = 0{\cdot}0425$. (a) Lift at $T = 0{\cdot}002$, (b) lift at $T = 0{\cdot}0125$, (c) lift at $T = 0{\cdot}03$, (d) lift at $T = 0{\cdot}075$; (e) drag at $T = 0{\cdot}002$, (f) drag at $T = 0{\cdot}0125$, (g) drag at $T = 0{\cdot}03$, (h) drag at $T = 0{\cdot}075$: ■, $l/D = 0$; +, 5; ∗, 10; □, 15; ×, 25; ⊠, 50.

5. CONCLUSION

Spanwise cross-correlation measurements of fluctuating pressures and of elemental fluctuating lift and drag forces on "long" cylinders have been made at subcritical Reynolds numbers over the range 10^4 to $2{\cdot}1 \times 10^5$ for blockage ratios 0·0425, 0·06 and 0·095 and for turbulence levels of 0·002, 0·0125, 0·03, 0·055 and 0·075. "Long" cylinder conditions exist when elemental r.m.s. force coefficients are independent of spanwise

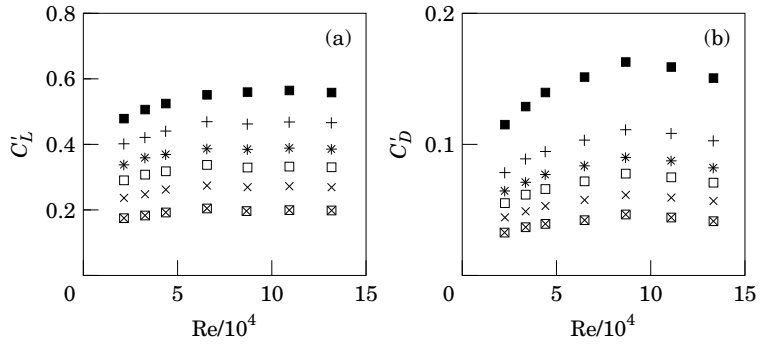

Figure 19. R.m.s. force coefficients for finite lengths of long cylinders at $B = 0{\cdot}06$. (a) lift at $T = 0{\cdot}002$, (b) drag at $T = 0{\cdot}002$; data symbols as in Figure 18.

location; they are achieved by use of suitable end plates with cylinder aspect ratios greater than about 10.

By numerical integration of the cross-correlation curves for elemental fluctuating lift and drag forces, conversion factors have been calculated which enable the r.m.s. force coefficients for finite lengths of "long" cylinders to be derived from previously measured elemental force coefficients. In this way, r.m.s. lift and drag coefficients have been calculated for lengths ranging from 5 to 50D for the range of parameters detailed above.

The spanwise cross-correlation coefficients for fluctuating pressure reported here are the first published which provide a complete description of the variation in correlation at all angular positions and for extensive ranges of blockage and of turbulence intensity in the approach flow. The results show that, in low turbulence flow, there is no measurable variation in the correlations with Reynolds number while the flow remains in the subcritical range and that the effects of blockage are very small over the range studied. Increases in turbulence in the approach flow cause substantial changes (reductions) in correlation coefficients, only when the flow exhibits characteristics of the early critical range. When this occurs, the spanwise correlation is reduced very much at angular positions downstream from separation, but there are relatively small changes for θ less than about 45°. The Reynolds number at which this occurs is reduced as the turbulence intensity is increased; it is $2{\cdot}1 \times 10^5$ when $T = 0{\cdot}0125$, $1{\cdot}1 \times 10^5$ when $T = 0{\cdot}03$ and $6{\cdot}6 \times 10^4$ when $T = 0{\cdot}075$.

The spanwise correlation coefficients for fluctuating lift and drag forces presented here are the first comprehensive set for a range of parameters; indeed, published data of this kind is very scarce. The results show that fluctuating lift is best correlated along the cylinder at the lower end of the subcritical range of Reynolds number and that the correlation deteriorates gradually as the Reynolds number is increased. Variation in blockage has small but not negligible effects. Increases in turbulence at the same Reynolds number cause the spanwise correlation to deteriorate. The changes are gradual and relatively small until the conditions are reached which cause large changes in the correlation of the fluctuating pressures, as discussed above. When this happens there is very rapid, substantial reduction in the spanwise correlation of fluctuating lift. The combinations of Reynolds number and turbulence intensity at which this change occurs are essentially the same as those detailed above for the large changes in fluctuating pressure correlations. The spanwise correlation of fluctuating drag is always much less than that of lift at the same conditions but it shows the same trends.

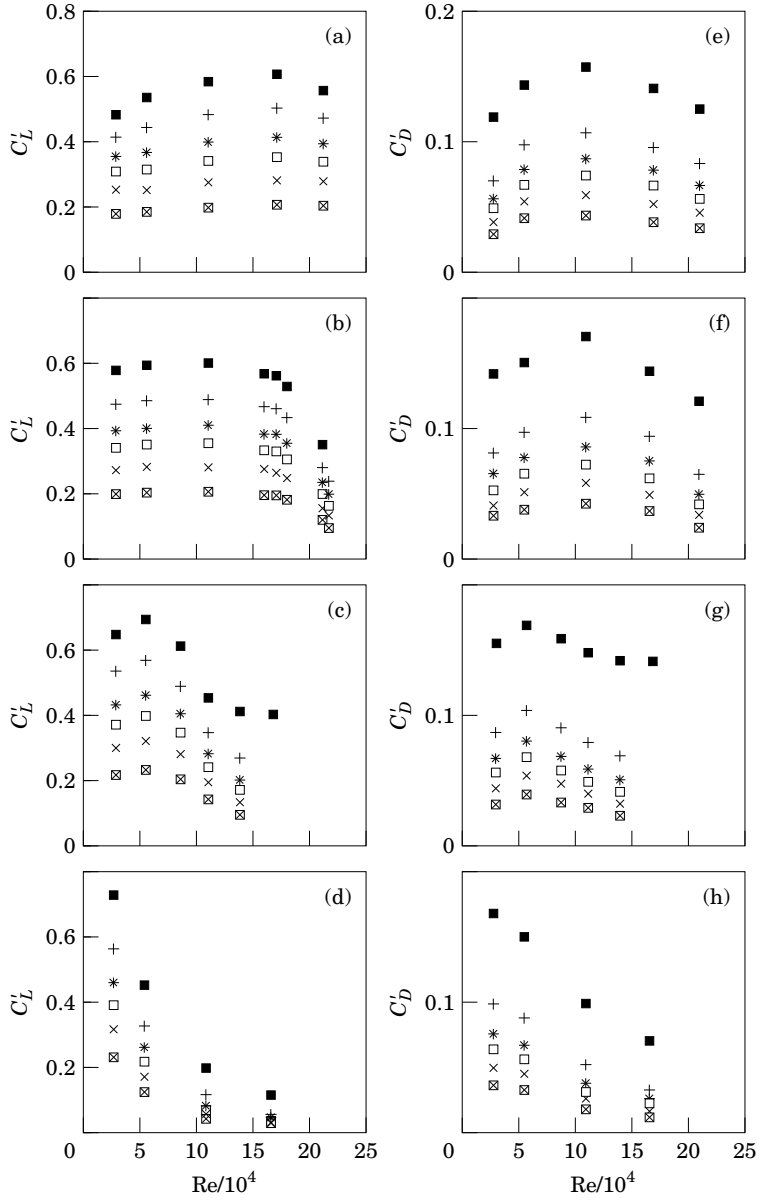

Figure 20. R.m.s. force coefficients for finite lengths of long cylinders at $B = 0{\cdot}095$. (a) Lift at $T = 0{\cdot}002$, (b) lift at $T = 0{\cdot}0125$, (c) lift at $T = 0{\cdot}03$, (d) lift at $T = 0{\cdot}075$; (e) drag at $T = 0{\cdot}002$, (f) drag at $T = 0{\cdot}0125$, (g) drag at $T = 0{\cdot}03$, (h) drag at $T = 0{\cdot}075$; data symbols as in Figure 18.

The r.m.s. force coefficients for finite lengths of "long" cylinders provide the first published comprehensive data set for the subcritical range of Reynolds numbers which includes the effects of variations in turbulence and blockage as well as variations in length. The results show that the r.m.s. force coefficients reduce most rapidly as the length over which they are averaged increases from 0 to $10D$. The decrease in lift coefficient in this range is approximately the same as occurs in the range 10 to $50D$. The r.m.s. drag coefficient decreases even more rapidly with increasing length than does the lift coefficient.

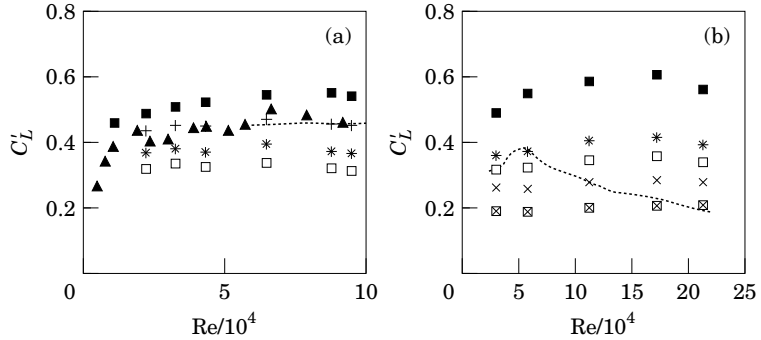

Figure 21. R.m.s. lift coefficients for finite lengths of cylinder. (a) This study at $B = 0{\cdot}0425$, $T = 0{\cdot}002$ compared with: ▲, Keefe (1961); - - - -, Cheung & Melbourne (1983). (b) This study at $B = 0{\cdot}095$, $T = 0{\cdot}002$ compared with: - - - -, Schewe (1983). Other data symbols as in Figure 18.

References

Batham, J. P. 1973 Pressure distributions on circular cylinders at critical Reynolds numbers. *Journal of Fluid Mechanics* **57,** 209–228.

Bruun, H. H. & Davies, P. O. A. L. 1975 An experimental investigation of the unsteady pressure forces on a circular cylinder in a turbulent flow. *Journal of Sound and Vibration* **40,** 535–559.

Cheung, C. K. & Melbourne, W. H. 1983 Turbulence effects on some aerodynamic parameters of a circular cylinder at supercritical Reynolds numbers. *Journal of Wind Engineering and Industrial Aerodynamics* **14,** 399–410.

Fox, T. A. & West, G. S. 1990 On the use of end plates with circular cylinders. *Experiments in Fluids* **9,** 237–239.

Frenkiel, F. N. 1949 The influence of the length of a hot wire on the measurement of turbulence. *The Physical Review* **75,** 1263–1264.

Kacker, S. C., Pennington, B. & Hill, R. S. 1973 Measurement of the fluctuating lift coefficient and of the correlation length of vortex shedding from cylindrical tubes. In *Proceedings UKAEA/NPL Symposium on Vibration Problems in Industry,* Keswick, UK.

Kacker, S. C., Pennington, B. & Hill, R. S. 1974 Fluctuating lift coefficient for a circular cylinder in cross flow. *I. Mech. E. Journal of Mechanical Engineering Science* **16,** 215–224.

Keefe, R. T. 1961 An investigation of the fluctuating forces acting on a stationary circular cylinder in a subsonic stream and of the associated sound field. UTIAS Report 76, University of Toronto, Toronto, Canada.

Kiya, M., Suzuki, Y. Arie, M. & Hagino, M. 1982 A contribution to the free-stream turbulence effect on the flow past a circular cylinder. *Journal of Fluid Mechanics* **115,** 151–164.

Novak, M. & Tanaka, H. 1975 Pressure correlations on a vibrating cylinder. In *Proceedings Fourth International Conference on Wind Effects on Buildings and Structures,* Heathrow, pp. 227–232, London: C.U.P.

Rebeiro, J. L. D. 1992 Fluctuating lift and its spanwise correlation on a circular cylinder in a smooth and in a turbulent flow: a critical review. *Journal of Wind Engineering and Industrial Aerodynamics* **40,** 179–198.

Schewe, G. 1983 On the force fluctuations acting on a circular cylinder in cross flow from subcritical up to transcritical Reynolds numbers. *Journal of Fluid Mechanics* **133,** 265–285.

Sonneville, P. 1976 Etude de la structure tridimensionelle des écoulements autour d'un cylindre circulaire. Bulletin de la Direction des Etudes et Recherches, Electricité de France, (A), No. 3.

Stansby, P. K. 1974 The effects of end plates on the base pressure coefficients of a circular cylinder. *Aeronautical Journal* **78,** 36–37.

Surry, D. 1972 Some effects of intense turbulence on the aerodynamics of a circular cylinder at sub-critical Reynolds numbers. *Journal of Fluid Mechanics* **52,** 543–563.

Szepessy, S. 1991 On the three-dimensionality of vortex shedding from a circular cylinder. Ph.D. thesis, Chalmers University of Technology, Sweden.

SZEPESSY, S. & BEARMAN, P. W. 1992 Aspect ratio and end effects on vortex shedding from a circular cylinder. *Journal of Fluid Mechanics* **234,** 191–217.

WEST, G. S. 1986 Experiments on circular cylinders in the sub-critical and transitional regimes with smooth and turbulent incident flow. Ph.D. thesis, The University of Queensland, Australia.

WEST, G. S. & APELT, C. J. 1993 Measurements of fluctuating pressure and forces on a circular cylinder in the Reynolds number range 10^4 to $2{\cdot}5 \times 10^5$. *Journal of Fluids and Structures* **7,** 227–244.

APPENDIX: NOMENCLATURE

A aspect ratio of cylinder between end plates ($= L/D$)
B area blockage ratio (model/wind tunnel)
C'_D r.m.s. fluctuating drag coefficient
C'_L r.m.s. fluctuating lift coefficient
D diameter of cylinder
e spanwise spacing in correlation measurements
f ratio of r.m.s. force coefficient for finite length of cylinder to elemental coefficient
L span of model between plates
l finite length part of a ''long'' cylinder
Re Reynolds number (based on D and U)
s_t turbulence scale
T turbulence intensity ($= u'/U$)
u' r.m.s. fluctuating velocity component in the flow direction
U mean velocity of approach flow
θ angular location in a cross-section measured from the stagnation point.
Λ correlation coefficient